Diffusion and microstructural properties of solutions of charged nanosized proteins: Experiment versus theory

J. Gapinski,[a] A. Wilk, and A. Patkowski
Institute of Physics, A. Mickiewicz University, 61-614 Poznan, Poland

W. Häußler
Forschungsneutronenquelle Heinz Maier-Leibnitz (FRM-II), Technische Universität München, D-85748 Garching, Germany

A. J. Banchio
Facultad de Matemática, Astronomía y Física, Universidad Nacional de Córdoba, Ciudad Universitaria, 5000 Córdoba, Argentina

R. Pecora
Chemistry Department, Stanford University, Stanford, California 94305-5080

G. Nägele
Institut für Festkörperforschung, Forschungszentrum Jülich, D-52425 Jülich, Germany

(Received 15 December 2004; accepted 15 June 2005; published online 11 August 2005)

We have reanalyzed our former static small-angle x-ray scattering and photon correlation spectroscopy results on dense solutions of charged spherical apoferritin proteins using theories recently developed for studies of colloids. The static structure factors $S(q)$, and the small-wave-number collective diffusion coefficient D_c determined from those experiments are interpreted now in terms of a theoretical scheme based on a Derjaguin-Landau-Verwey-Overbeek-type continuum model of charged colloidal spheres. This scheme accounts, in an approximate way, for many-body hydrodynamic interactions. Stokesian dynamics computer simulations of the hydrodynamic function have been performed for the first time for dense charge-stabilized dispersions to assess the accuracy of the theoretical scheme. We show that the continuum model allows for a consistent description of all experimental results, and that the effective particle charge is dependent upon the protein concentration relative to the added salt concentration. In addition, we discuss the consequences of small ions dynamics for the collective protein diffusion within the framework of the coupled-mode theory. © *2005 American Institute of Physics*. [DOI: 10.1063/1.1996569]

I. INTRODUCTION

Recently, some of us have used a paracrystalline theory to analyze the data obtained from small-angle x-ray scattering (SAXS), and the coupled-mode theory to analyze the data from photon correlation spectroscopy (PCS) studies of low-salt solutions of apoferritin.[1] Since the dynamic data are not accessible by PCS in the vicinity of the primary peak in the static structure factor, neutron spin-echo (NSE) studies were performed on the same system,[2,3] but in a much narrower range of volume fractions and added salt content.

In the present work, we reanalyze the SAXS data for the static structure factor, and the PCS and NSE data for collective diffusion in terms of a one-component model of dressed spherical macroions. In this model the protein interactions are simply described by a Derjaguin-Landau-Verwey-Overbeek(DLVO)-type screened Coulomb potential characterized by an effective particle charge and an electrostatic screening parameter. In the framework of this model, the Rogers-Young[4] (RY) and the rescaled mean-spherical approximation[5] (RMSA) integral equation schemes are used to fit the apoferritin structure factors determined by SAXS, and to deduce the concentration dependence of the effective charges. Collective diffusion[6–8] is determined both by direct and by solvent-mediated hydrodynamic interactions (HIs). For the rather dense solutions of apoferritin studied in Ref. 1, one needs to account for HI beyond the pairwise-additive level. For this reason we calculate in this work the collective diffusion coefficient using a so-called $\delta\gamma$ scheme, which accounts, in an approximate way, for many-body HI. Novel accelerated Stokesian dynamics (ASD) computer simulations of short-time self- and collective properties are performed to assess the accuracy of this scheme for its application to dense charge-stabilized dispersions. The $\delta\gamma$ scheme is used subsequently to explain the volume fraction dependence, and the ionic-strength dependence, of the PCS-measured collective diffusion coefficients. Furthermore this scheme is used to interpret NSE data for the wave-number-dependent collective diffusion coefficient. As a major result it will be shown that the experimental data can be consistently described on the basis of the one-component macroion-fluid (OMF) model. The coupling of the collective diffusion of proteins to

[a]Author to whom corespondence should be addressed. Electronic mail: gapinski@amu.edu.pl

TABLE I. Parameters used in the RY and RMSA fits to the SAXS-measured $S(q)$, for five differently concentrated samples of apoferritin in 10-μM NaCl solution. The effective protein charge numbers Z_{RY} and Z_{RMSA} have been determined from a fit to the experimental peak heights of $S(q)$. Here, $\sigma=13.8$ nm is the hydrodynamic protein diameter used in all model calculations, and $T=293.16$ K and $\epsilon=80.36$ are the temperature and dielectric constant of water corresponding to $L_B=0.71$ nm. Moreover, ϕ is the protein volume fraction determined by the hydrodynamic particle radius, C_w is the protein weight concentration, and $\langle r\rangle=n^{-1/3}$ is the geometric mean particle distance; κ_{RMSA} and κ_{RY} are the screening parameters calculated according to Eq. (2), with Z as obtained from the RMSA and Rogers-Young fits, respectively. Note that the effective protein charges used in our ASD and RY calculations are identical.

Sample	C_w(g/l)	ϕ	$\langle r\rangle/\sigma$	Z_{RMSA}	$\sigma\cdot\kappa_{RMSA}$	$Z_{RY\text{-}ASD}$	$\sigma\cdot\kappa_{RY}$
1	259	0.358	1.135	55	6.151	39	5.179
2	237	0.327	1.169	49	5.426	36	4.652
3	200	0.276	1.238	48	4.757	37	4.177
4	160	0.221	1.333	42	3.836	34.5	3.478
5	111	0.153	1.506	22	2.222	20.5	2.144

the noninstantaneous dynamics of the counter- and coions will be discussed on the basis of the coupled-mode theory (CMT). This discussion includes a critical analysis of the validity of the CMT.

Section II describes the OMF model, and includes some details on the theoretical and computer simulation methods employed in this work. This section further summarizes some known results about short-time collective and self-diffusion in dispersions of charged or neutral colloidal spheres. The experimental setup, methods, and the data handling are described in Sec. III. In Sec. IV, the theoretical methods are applied to interpret the SAXS, PCS, and NSE data, and the density dependence and ionic-strength dependence of the effective protein charges are inferred and discussed. In Sec. V, we conclude the paper by a short discussion of the main results.

II. A ONE-COMPONENT MODEL OF CHARGED PROTEIN SOLUTIONS

Our theoretical calculations of static and dynamic properties of apoferritin protein solutions are based on the OMF model. In this continuum model, the globular proteins are described as uniformly charged hard spheres, interacting by the effective, i.e., state-dependent, pair potential[8–10]

$$\frac{u(r)}{k_BT}=L_BZ^2\left(\frac{e^{\kappa a}}{1+\kappa a}\right)^2\frac{e^{-\kappa r}}{r},\quad r>2a. \tag{1}$$

Equation (1) is the repulsive part of the celebrated DLVO pair potential. It can be derived on the basis of the linearized Poisson-Boltzmann theory[9] or the (linear) mean-spherical approximation on assuming pointlike counter- and coions (see, e.g., Ref. 8).

For nonweakly charged macroions (proteins), Z needs to be interpreted as an *effective* protein (i.e., macroion) charge number, which accounts to some extent for nonlinear screening effects. The effective macroion charge used in the OMF model must then be distinguished from the *bare* protein charge as specified within the primitive model where both macroions and microions (i.e., counterions and electrolyte ions) are treated on equal footing as uniformly charged hard spheres. The effective protein charge number Z is typically smaller than the bare one. They become equal only in the limit of weak ionic interactions.[11–13] Moreover, a is the hard-core radius of a sphere, and $L_B=e^2/(\epsilon k_BT)$ is the Bjerrum length for a suspending fluid of dielectric constant ϵ. In water at room temperature, $L_B=0.71$ nm. The fluid is thus modeled as a continuum, characterized for the statics only by ϵ, and dynamically only in terms of the fluid shear viscosity η_0. The electrostatic screening parameter, κ, is given by

$$\kappa^2=\frac{4\pi L_B[n|Z|+2n_s]}{1-\phi}=\kappa_{ci}^2+\kappa_s^2, \tag{2}$$

where n is the protein (i.e., macroion) number density, n_s is the number density of possibly added 1-1 electrolyte, and $\phi=(4\pi/3)na^3$ is the protein volume fraction. We note that κ^2 comprises a contribution, κ_{ci}^2, due to counterions, which are assumed here to be monovalent, and a contribution, κ_s^2, arising from the added electrolyte (e.g., NaCl).

The factor $1/(1-\phi)$ corrects for the free volume accessible to the screening counterions and electrolyte ions due to the presence of the macroions. The occurrence of the free volume factor in the expression for κ has been discussed in Refs. 10, 14, and 15. It is of relevance only for very dense dispersions. For the protein solutions discussed in this work we have found that the reduced volume correction is practically negligible in its influence on the calculated static structure factors and hydrodynamic functions, even when the largest volume fraction $\phi\approx0.36$ is considered (cf. Table I).

The OMF model ignores the discreteness (and separate dynamics) of the mobile counter- and coions, as well as the discreteness of the charge distribution on the protein surfaces. Moreover, van der Waals dispersion forces, solvent hydration forces, and possible short-ranged hydrophobic protein attractions are not included in this model. Nonetheless, Eq. (1) constitutes in general a good approximation for the effective pair potential of strongly charged colloidal particles. Using the state-dependent pair potential of Eq. (1) amounts to ignore, even for renormalized interaction parameters, possible N-body potential contributions ($N>2$) to the static and dynamic correlation functions (see, e.g., Refs. 16,17).

In the present joint experimental-theoretical work, we do not attempt to assess the importance of many-body potential contributions which might lead to deviations from the

Yukawa-fluid-like OMF model, nor do we want to discuss possible relationships between bare and effective macroion charges (and associated screening parameters). Only approximate answers to these challenging problems have been found to date, and existing results depend significantly on the invoked approximations (e.g., various density-functional theories and Poisson-Boltzmann-type approaches), and on simplifying model assumptions (e.g., on the use of a single macroion cell model or a jellium model). For apoferritin solutions we will address these problems in future work.

The main objective of the present study is to investigate to what extent the OMF model is useful, in spite of its severe simplifications, for a *consistent* description of the statics and, in particular, of the dynamics of charge-stabilized protein solutions at low to moderate salinities.

While the OMF model is applicable with good success to charge-stabilized colloidal dispersions of strongly charged particles typically a few hundred nanometers in size, the discrete nature of microions and of surface charges should be more important in the case of less charged and nanosized proteins. Indeed, recent molecular-dynamics simulations of Allahyarov *et al.*,[18] of a refined primitive model of proteins with discrete surface charge patterns, reveal profound differences to the OMF model both for the osmotic second virial coefficient and for the protein pair forces. However, these differences become strong only for very large ionic strengths of 1-2M. In contrast, the added salt concentration in the apoferritin solutions in the SAXS, PCS and NSE experiments discussed in this work is significantly below $10^{-3}M$.

From SAXS experiments and from the knowledge of the single protein form factor, one can determine the static structure factor, $S(q)$, of the globular proteins, for scattering wave numbers q extending up to the second maximum. The static structure factor is related to radial distribution function, $g(r)$, by[19]

$$g(r) = 1 + \frac{1}{2\pi^2 n\, r}\int_0^\infty dq\; q\, \sin(qr)[S(q) - 1]. \tag{3}$$

The function $g(r)$ quantifies the conditional probability of finding a protein at a distance r from any other one. To calculate $S(q)$ and $g(r)$ from the OMF pair potential in Eq. (1), we solve the Ornstein-Zernike integral equation for one-component systems in combination with the well-established RY and (RMSA) closure schemes.[4,5,8,20] Comparisons with Monte Carlo computer simulations show that the partially thermodynamically self-consistent RY scheme is quite accurate within the three-dimensional OMF model.[8,20] Its disadvantage is that it is numerically far more complicated than the semianalytical RMSA solution. Interestingly enough, the RMSA leads in most cases to nearly identical results for $S(q)$ and $g(r)$ as the RY scheme, provided a somewhat larger value of Z is used in the RMSA calculations (cf. Table I). A detailed account on the properties of various integral equation schemes including the RMSA and RY is provided in Refs. 8,20.

PCS gives information on spatial and temporal correlations between local fluctuations in the protein concentration. The key quantity determined in PCS experiments on spherical particles is the dynamic structure factor

$$S(q,t) = \left\langle \frac{1}{N}\sum_{l,j=1}^{N} \exp\{i\mathbf{q}\cdot[\mathbf{R}_l(0) - \mathbf{R}_j(t)]\}\right\rangle. \tag{4}$$

In this formula, N is the number of proteins within a macroscopically large scattering volume, $\mathbf{R}_j(t)$ is the position vector pointing to the center of the jth particle at time t, $\mathbf{q}$ is the scattering vector, and $\langle\cdots\rangle$ denotes an equilibrium ensemble average. At short times, $S(q,t)$ decays exponentially according to[6,8,9,21]

$$\frac{S(q,t)}{S(q)} \approx \exp[-q^2 D_c(q)t], \quad \tau_B \ll t \ll \tau_I, \tag{5}$$

with a wave-number-dependent (short-time) collective diffusion coefficient $D_c(q)$. Here, $\tau_B = MD_0/k_BT$ is the relaxation time for the momentum of an isolated protein sphere of mass M, and diffusion coefficient $D_0 = k_BT/(6\pi\eta_0 a)$. A sphere requires roughly the time $\tau_I = a^2/D_0$ to diffuse a distance equal to its own hydrodynamic radius a. In principle, one should distinguish between the hydrodynamic radius a and the excluded volume radius appearing in Eq. (1), however, the difference is usually small. For protein spheres in water with $a = 6.9$ nm, one finds $\tau_B \approx 0.01$ ps and $\tau_I \approx 1.53$ μs.

In conventional PCS experiments like ours, only times much larger than τ_B are resolved. The diffusion of the proteins for $t \gg \tau_B$ is governed by the many-body Smoluchowski equation. This time evolution equation for the many-sphere probability density describes the relaxation of the particle positions under the presence of direct interactions [cf. Eq. (1)] and quasi-instantaneous hydrodynamic forces.[7] By assuming an unstructured fluid on the length scale of the proteins, the hydrodynamic interactions can be described by the creeping flow equations of slow and incompressible fluid flow, using (stick) boundary conditions on the sphere surfaces.[7,8]

Within the Smoluchowski dynamics of overdamped particle motion, $D_c(q)$ can be expressed as[8]

$$D_c(q) = D_0 \frac{H(q)}{S(q)}, \tag{6}$$

where $S(q) = S(q, t=0)$ is the static structure factor. The hydrodynamic function, $H(q)$, contains the influence of the HI on the short-time collective diffusion. It is the sum of a q-independent self- and a q-dependent distinct part according to

$$H(q) = \frac{D_s}{D_0} + H_d(q), \tag{7}$$

where D_s is the translational short-time self-diffusion coefficient. The coefficient D_s quantifies the initial slope, for $\tau_B \ll t \ll \tau_I$, of the particle mean-squared displacement $W(t)$, which is defined in three dimensions as

$$W(t) = \tfrac{1}{6}\langle[\mathbf{R}(t) - \mathbf{R}(0)]^2\rangle. \tag{8}$$

Without HI acting among the proteins, $H(q)=1$, corresponding to $D_s=D_0$ and $H_d(q)=0$. Any nonconstant $H(q)$ is thus a signature of hydrodynamically interacting particles. Due to the small size of the apoferritin proteins as compared to the wavelengths of visible light, only the small-wave-number regime is covered by PCS. For $qa \ll 1$, $H(q)$ reduces to the short-time (relative) sedimentation velocity, U_s, of slowly sedimenting spheres, viz.,[9,20]

$$\lim_{q\to 0} H(q) = \frac{U_s}{U_0}, \tag{9}$$

where U_0 is the sedimentation velocity at infinite dilution. Furthermore, $D_c(q)$ reduces for $qa \ll 1$ to the short-time collective diffusion coefficient, D_c, given by

$$D_c = \frac{D_0}{S(0)}\frac{U_s}{U_0}. \tag{10}$$

In the opposite limit of $qa \gg 1$ which is not accessible to PCS, $H(q)$ becomes equal to D_s/D_0.

The correlation times of $t=100$ μs for dilute systems, and $t=10$ μs for dense and low-salt systems, which we have selected in our PCS experiments, are much larger than τ_I. As a consequence, memory effects due to dynamic particle caging play a role in general.[6] This is certainly the case for self-diffusion, where the long-time self-diffusion coefficient can be substantially smaller than the short-time one [cf. our Stokesian dynamics simulations for the mean-squared displacement $W(t)$ in Sec. IV]. With regard to collective diffusion, however, memory effects are quite small in the small-wave-number regime $qa \ll 1$, even for concentrated dispersions with strong many-body HI. The long-time sedimentation velocity, U_l, measured in macroscopic sedimentation experiments at times $t \gg \tau_I$, is therefore only slightly smaller than U_s (the differences are less than 6% even for the case of very concentrated hard spheres[22,23]). In systems with strong two-body far-field HI contributions and negligibly small lubrication forces such as dilute or moderately dense charge-stabilized dispersions, the long-time and short-time sedimentation velocities and, likewise, the short-time and long-time collective diffusion coefficients become practically equal.

Whereas PCS measurements on the small apoferritin molecules are limited to the small-q regime, using NSE one can determine the dynamic structure factor for a range of wave numbers extending well beyond the location, q_m, of the primary peak of the static structure factor $S(q)$. For finite q, the dynamic structure factor of interacting particles decays in general nonexponentially at long times $t \gg \tau_I$. An important exemption is the exponential long-time decay of $S(q,t)$ observed for $q \approx q_m$. This collective long-time mode is related to collective rearrangements in the dynamic cages of next-neighbor particles. The long-time mode disappears for weakly interacting particles systems where the dynamic caging effect is not strong enough.[24] It should be noted, however, that the maximum spin-echo times in today's NSE spectrometers are well below the interaction time $\tau_I \approx 1.5$ μs of appoferritin.[3] Therefore, NSE measurements allow us to determine the wave-number-dependent short-time collective diffusion coefficient $D_c(q)$. In combination with SAXS or SANS measurements of $S(q)$, one can then determine the hydrodynamic function $H(q)$.

The volume fractions, ϕ, of our apoferritin samples (i.e., $\phi=0.15-0.36$) are so large that one needs to consider three-body and higher-order HI contributions, in addition to the long-range and pairwise-additive far-field contributions. In this work, we treat the many-body HI in an approximate way using a renormalization scheme developed by Beenakker and co-worker.[25,26] This method is based on an expansion of $H(q)$ in powers of renormalized density fluctuations, commonly referred to as the $\delta\gamma$ expansion method. It has been applied originally only to hard spheres.[25,26] Following earlier work on its application to dispersions of charged colloidal spheres,[8,27–30] we evaluate the $\delta\gamma$ expansion to zeroth order. The zeroth-order $\delta\gamma$ method requires only the static structure factor as input. The latter is obtained from the RY or, likewise, from the RMSA integral equation scheme. The lengthy expression for $H(q)$ in the zeroth-order $\delta\gamma$ approximation has been given and discussed in Ref. 27. Therefore, it will not be repeated here.

The accuracy of the $\delta\gamma$ method had been assessed to date only for monodisperse hard-sphere suspensions. Lattice-Boltzmann simulations[31,32] and detailed Stokesian dynamics simulations[33] of hard-sphere hydrodynamic functions have shown that the $\delta\gamma$ method works rather well for volume fractions up to $\phi \leqslant 0.3$. Far less is known, instead, about its accuracy in the case of (dense) charge-stabilized dispersions. For this reason, and for the first time, we have performed ASD simulations of $H(q)$ within the OMF model of charged spheres. Our simulations are based on an accelerated simulation algorithm for Brownian systems developed very recently by Banchio and Brady.[34] For computing $H(q)$ using ASD, equilibrium configurations of spheres were obtained using a Monte Carlo simulation code for charged spheres, and a molecular-dynamics simulation code for neutral hard spheres. The HIs were then computed using the ASD scheme. Here we will only discuss a few results of these simulations relevant to the PCS measurements of D_c for apoferritin. A full account of the short-time ASD simulation results for charge-stabilized and neutral colloidal dispersions will be given in a separate article.[33] In this separate article, we will further address the controversial issue of hydrodynamic screening, apparently observed in dynamic x-ray measurements of $H(q)$ for moderately dense suspensions of charged silica spheres.[35–38]

We conclude this section on theoretical methods by quoting a few salient results on collective diffusion coefficients known for hard-sphere and for charge-stabilized dispersions. For hard spheres with $\phi \leqslant 0.5$, the principal peak value, $H(q_m)$, of $H(q)$ at q_m is well described by[20,39]

$$H(q_m) = 1 - 1.35\phi. \tag{11}$$

By combining this result with another empirical expression, viz.,[24]

$$S(q_m) = 1 + 0.644\phi\frac{(1-0.5\phi)}{(1-\phi)^3}, \tag{12}$$

for the peak height of the hard-sphere static structure factor, which is valid to very good accuracy for $\phi \leqslant 0.5$,[24] one obtains an analytical expression for $D_c(q_m)$. This expression for $D_c(q_m)$ is in perfect agreement with PCS data of $D_c(q_m)$ for hard-sphere dispersions,[40] and with lattice-Boltzmann simulation data of $D_c(q_m)$ and $H(q_m)$ by Segrè *et al.*[32]

Recently, a truncated virial expansion of the short-time sedimentation coefficient of hard spheres up to quadratic order in ϕ has been derived by Cichocki *et al.* The expansion reads explicitly[41]

$$H(0) = 1 - 6.546\phi + 21.918\phi^2 + \mathcal{O}(\phi^3). \tag{13}$$

In combination with the virial expansion, $S(0)=1-8\phi+34\phi^2+\mathcal{O}(\phi^3)$, for the relative osmotic compressibility of hard spheres, one obtains the result[20]

$$\frac{D_c}{D_0} = 1 + 1.454\phi - 0.45\phi^2 + \mathcal{O}(\phi^3) \tag{14}$$

for the (short-time) collective diffusion coefficient of hard spheres, indicating that $D_c > D_0$.[20] The modest increase in D_c with ϕ, as described by Eq. (14) for smaller ϕ, is opposed by the HI through the factor $H(0)$, which causes D_c to further increase rather slowly for large values of ϕ.[32]

Contrary to hard spheres, for dispersions of strongly charged spheres at low salinity there is no regular virial expansion in terms of ϕ for diffusional transport coefficients.[8] In these charge-stabilized systems, the peak height of $H(q)$ is well approximated, for small densities $\phi \leqslant 10^{-2}$, by the nonlinear form[39]

$$H(q_m) \approx 1 + p_m\phi^{0.4}, \tag{15}$$

with a coefficient $1 \leqslant p_m \leqslant 1.5$ which is only weakly dependent on the particle size and charge.[39,42] Equation (15) states that, for low concentrations, $H(q_m)$ is monotonically increasing in ϕ. However, for moderate particle charges, $H(q_m)$ will reach a maximum within the fluid-phase regime, with a consecutive attenuation upon further increasing ϕ (cf. Ref. 33).

In the small-q limit, and for $\phi \leqslant 0.05$, the short-time sedimentation coefficient of charge-stabilized spheres reads[8]

$$H(0) \approx 1 - p_0\phi^{1/3}, \tag{16}$$

with a coefficient $p_0 \approx 1.8$ which is nearly constant. The nonlinear concentration dependence of the short-time coefficients $H(0)$ and $H(q_m)$, quantified by Eqs. (15) and (16), respectively, arises from the $\phi^{-1/3}$ dependence of the location, $r_m(\phi)$, of the principal peak of $g(r)$ for strongly charged and de-ionized particle dispersions.[8,42] In this special case of dilute dispersions of strongly charged particles dominated by counterion screening, it is sufficient to account only for the leading-order two-body contributions to the translational hydrodynamic mobility functions up to the third order in the inverse interparticle distance expansion. This leads to the expression[8,28]

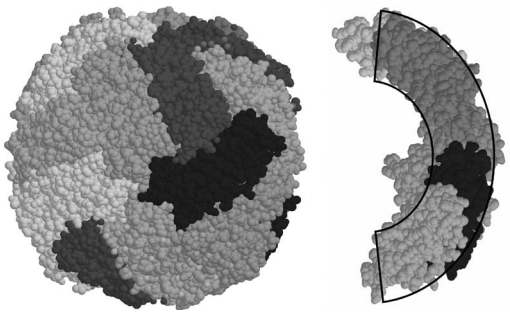

FIG. 1. Schematic view of an apoferritin protein. The differently shaded regions are the peptide subunits. The figure on the right is a cut through a portion of the protein shell.

$$H(q) = 1 - 15\ \phi\frac{j_1(y)}{y} + 18\ \phi\int_1^\infty dx\ x[g(x)-1] \times\left(j_0(xy) - \frac{j_1(xy)}{xy} + \frac{j_2(xy)}{6x^2}\right), \tag{17}$$

where $y=2qa$, $x=r/(2a)$, and j_n is the spherical Bessel function of order n. Experimental results for the hydrodynamic functions of aqueous dispersions of strongly charged polymer spheres[43] are very well described by Eq. (17).

III. SAXS AND PCS ON CONCENTRATED APOFERRITIN SOLUTIONS

A schematic view of an apoferritin protein is given in Fig. 1. The peptide subunits in the protein shell are differently shaded. The figure on the right shows a cut through a portion of the shell. From the point of view of colloidal science, apoferritin is a very nice monodisperse model system of small and spherically shaped particles which, under proper conditions, can acquire a high surface charge density. Apoferritin solutions are perfectly monodisperse and relatively stable, i.e., for weeks at room temperature and even for months at 4 °C. The hydrodynamic radius measured by PCS is 6.9 nm,[1] which corresponds to $D_0 = 3.11 \times 10^{-7}$ cm^2/s (for water at 20 °C).

The details of the sample preparation of apoferritin solutions and experimental setups have been already given elsewhere,[1] hence here we give only a brief description. Desired buffering conditions were obtained through dialysis of the bulk horse spleen apoferritin solution (SIGMA) to aqueous solutions of various sodium chloride concentrations. The small-angle x-ray scattering measurements were performed by means of a Kratky camera (Kratky Compact, Paar, Austria) at a wavelength of 1.54 Å (Cu K_α) using a position sensitive detector (Braun). The ultrasmall-angle x-ray scattering measurements were performed at the European Synchrotron Radiation Facility (ESRF Grenoble, ID10). The monochromatized beam ($\lambda = 1.55$ Å, $\Delta E/E = 6 \times 10^{-5}$) was collimated by means of a 10-μm pinhole. The scintillation detector was mounted at a distance of 2.275 m behind the sample.

The form-factor measurements required to calculate the structure factor functions were performed for a sample concentration of 100 g/l in 100-mM NaCl solution to screen electrostatic interactions. The shell model was applied to fit

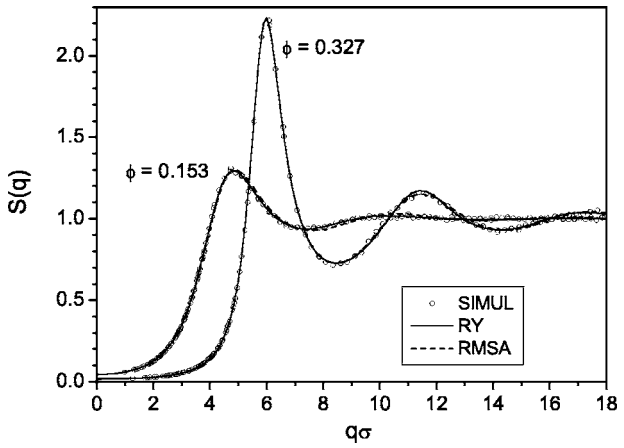

FIG. 2. Static structure factor $S(q)$ vs $q\sigma$ for two charge-stabilized systems of volume fractions $\phi=0.327$ (sample 2: upper curve) and $\phi=0.153$ (sample 5: lower curve), respectively. The ASD simulation results (open circles) are compared with the RY (solid lines) and RMSA (dashed lines) predictions for $S(q)$. The system parameters L_B, σ, and n_s and effective charge numbers Z of samples 2 and 5 entering the pair potential in Eqs. (1) and (2) are listed in Table I. In particular, $Z_{\mathrm{ASD}}=Z_{\mathrm{RY}}=36$ and $Z_{\mathrm{RMSA}}=49$ for $\phi=0.327$, and $Z_{\mathrm{ASD}}=Z_{\mathrm{RY}}=20.5$ and $Z_{\mathrm{RMSA}}=22$ for $\phi=0.153$. Note that the charge-adjusted RMSA structure factors are nearly indistinguishable from the RY structure factors.

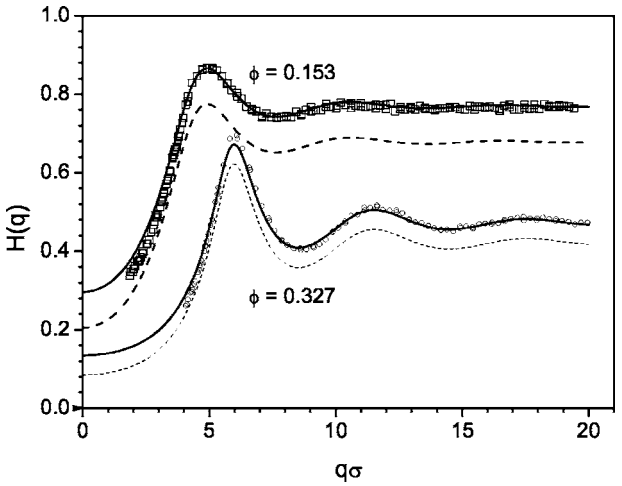

FIG. 3. Finite-sized adjusted ASD results (symbols), and zeroth-order $\delta\gamma$ approximation results (dashed lines), with RY input for $S(q)$ for the hydrodynamic function $H(q)$, corresponding to samples 2 and 5 in Fig. 2. The lower set of curves is for $\phi=0.327$, the upper one for $\phi=0.153$. All systems parameters are equal to the parameters used in Fig. 2 for the ASD and RY results. The solid curves are hybrid $\delta\gamma$-ASD results for $H(q)$, with $D_s^{\delta\gamma}/D_0=0.42$ replaced by $D_s^{\mathrm{ASD}}/D_0=0.47$ for $\phi=0.327$, and $D_s^{\delta\gamma}/D_0=0.68$ replaced by $D_s^{\mathrm{ASD}}/D_0=0.77$ for $\phi=0.153$.

the high-q (oscillating) part of the spectrum not affected by the hard-sphere static structure factor, which at this concentration deviates substantially from unity in the low-q range.

For the photon correlation spectroscopy measurements we used a krypton-ion laser (Spectra Physics, USA, $\lambda=647$ nm), a goniometer and a digital correlator (ALV GmbH, Germany), and a high quantum efficiency avalanche photodiode (SPCM-PQ from EG&G, Canada, specially selected).

Due to residual absorption of the laser light at the wavelength used we reduced the beam path in the sample to 1 mm and the measurements were performed as a function of the incident-beam intensity. As has been reported in Ref. 1, at low added salt concentrations an additional slow mode was always present with characteristic times corresponding to hydrodynamic radii between 40 and 100 nm. Therefore, the time correlation functions have been fitted with a two-exponential model, and the shorter decay times have been used to calculate the apoferritin diffusion coefficients. For more details on our analysis of the slow mode process, we refer to Ref. 1.

IV. RESULTS AND DISCUSSION

Using the one-component macroion-fluid model of charged globular proteins, we first assess the degree of accuracy of the zeroth-order $\delta\gamma$ approximation and of the RY and RMSA static inputs, by a comparison with accelerated SD simulations of $H(q)$ and $S(q)$. To the best of our knowledge, the Stokesian dynamics simulation results of $H(q)$ presented here are the only ones available so far for (dense) charge-stabilized dispersions with strong many-body HI. Consequently this amounts to the first quantitative test of the $\delta\gamma$ scheme in its application to dense charge-stabilized dispersions. In the second part of this section, our OMF-based theoretical methods are applied to experimental static structure factor and collective diffusion data on moderately salted apoferritin solutions.

A. OMF results: theory versus computer simulations

1. Static structure factor

In Fig. 2, RY and RMSA results for the static structure factor at two different volume fractions, $\phi=0.327$ (sample 2 in Table I) and $\phi=0.153$ (sample 5 in Table I), are compared with the corresponding accelerated Stokesian dynamics simulation results. The system parameters used in the RY calculations for the structure factors of samples 2 and 5 are listed in Table I. In our ASD simulations we have used identical parameters as for the RY calculations. As seen, the RY-$S(q)$ practically coincides with simulation data within the displayed q range. The RMSA requires somewhat larger values of the effective charge to match the peak heights of the ASD structure factors. This is due to the well-known fact that the RMSA underestimates the pair correlations in dispersions of strongly correlated particles. However, once the RMSA effective charge has been adjusted accordingly, very good agreement is found with the corresponding RY structure factor (cf. Fig. 2).

2. Hydrodynamic function

To correct for finite-size effects arising from the periodic boundary conditions, the ASD simulations of the hydrodynamic function $H(q)$ have been repeated for $N=125$, 216, 512, and 860 particles. The extrapolation to the thermodynamic limit is then obtained using the finite-size scaling form

$$H(q) = H_N(q) + 1.76\, S(q;\phi)\frac{\eta_0}{\eta_\infty(\phi)}(\phi/N)^{1/3}, \tag{18}$$

originally proposed for hard-sphere systems by Ladd and co-workers.[31,44] Here, $\eta_\infty(\phi)$ is the high-frequency limiting shear viscosity of the suspension at zero Peclet number. Finite-size scaling of the ASD-$H(q)$ requires thus, in addition, the calculation of the viscosity $\eta_\infty(\phi)$ of charge-stabilized dispersions. Our simulation results for the various N neatly collapse on a single master curve when Eq. (18) is applied. The master curve is identified with the finite-size corrected $H(q)$.

Figure 3 displays our ASD data of $H(q)$ for the systems 2 and 5 discussed in Fig. 2. The dashed lines are the corresponding zeroth-order $\delta\gamma$-scheme results with RY input, for the same input parameters as used in the ASD simulations. While the oscillations in the q dependence of $H(q)$ are very well captured by the $\delta\gamma$ scheme, the ASD-$H(q)$ is overall underestimated. The reason for this feature is that the $\delta\gamma$ scheme approximates the self-part, D_s/D_0, of $H(q)$ more severely than the distinct part [cf. Eq. (7)]. In the zeroth-order $\delta\gamma$ approximation, D_s is determined solely by the volume fraction ϕ, independent of the particle charge and the screening parameter, whereas the $\delta\gamma$-$H_d(q)$ depends also on the form of the radial distribution function [cf., e.g., Eqs. (5) and (11) in Ref. 27]. As a consequence, the accuracy of the $\delta\gamma$ scheme is improved when accurate simulation data are used instead for the self-part of $H(q)$, leading to an upward shift of $\delta\gamma$-$H(q)$ by a value of $(D_s^{\mathrm{ASD}} - D_s^{\delta\gamma})/D_0$. The good overall agreement between simulation data and the $\delta\gamma$ scheme for $H_d(q)$ combined with a simulation input for D_s is illustrated in Fig. 3. The good accuracy of this hybrid $\delta\gamma$ scheme had been realized already in its earlier applications[8,27] to dilute charge-stabilized dispersions of coated silica spheres.[45] For those colloidal systems, D_s can be obtained analytically with good accuracy using a pairwise-additive approximation for the hydrodynamic interactions as detailed in Refs. 8,28.

Contrary to dilute suspensions of strongly charged colloidal particles at low salinities, where the principal peak, $H(q_m)$, of $H(q)$ is larger than one, and where the peak increases monotonically in ϕ as described by Eq. (15), the $H(q_m)$ for the apoferritin solutions under consideration lies below one and decreases in height with increasing ϕ. The latter behavior of $H(q)$ is, in fact, typical for suspensions of colloidal hard spheres with their strong many-body HI. The effective charges of the apoferritin molecules are rather modest but, due to the small apoferritin size, the surface charge densities are quite high by colloid standards. However, the particle volume fractions are quite large (cf. the Table I) which implies that the particles can approach each other quite closely [cf. Fig. 6 for a typical $g(r)$]. Many-body HI effects thus come into play, and this explains the similarity with hard-sphere systems for the concentration dependence of $H(q_m)$.

To analyze in more detail the similarity with dispersions of neutral spheres, in Fig. 4 we compare the hydrodynamic functions of apoferritin solutions (within the OMF model) with the $H(q)$ of neutral hard spheres at the same volume fraction. The principal peak height of the ASD-$H(q)$ for neutral spheres is consistently located below that of charged spheres, and its location is shifted to a larger wave number. This is a generic behavior which we have observed for all systems. It is related to the fact that the first-neighbor shell part of the hard-sphere $g(r)$ is less pronounced than for the corresponding charged-sphere system, and that the shell is located at somewhat smaller interparticle distances. Recall here from Eq. (11) that the $H(q_m)$ of hard spheres is well described by a linear ϕ dependence. The value -1.35 of the slope has been confirmed by our most recent ASD simulations.[33] The $\delta\gamma$-scheme predictions for the hard-sphere $H(q)$ are rather close to the simulation data for $0.05 < \phi < 0.3$, although the peak height is slightly underestimated. However, the $\delta\gamma$ scheme significantly overestimates the hard-sphere $H(q_m)$ in the case of very dense hard-sphere dispersions with $\phi > 0.4$.[33] For the volume fractions of samples 2 and 3 considered in Fig. 4, $D_s^{\mathrm{ASD,HS}}/D_0 \approx 0.42$ for $\phi = 0.327$ and $D_s^{\mathrm{ASD,HS}}/D_0 \approx 0.72$ for $\phi = 0.153$. These values are fairly close to the corresponding $\delta\gamma$-scheme predictions $D_s^{\delta\gamma,\mathrm{HS}}/D_0 \approx 0.42$ and $D_s^{\delta\gamma,\mathrm{HS}}/D_0 \approx 0.68$, respectively, for hard spheres. Similar to the case of charged particles, the $\delta\gamma$ scheme is slightly improved when simulation inputs for D_s are used. We note here that the short-time self-diffusion coefficient of hard spheres is rather well parametrized, when compared to experimental data for $0 < \phi < 0.5$,[20] by the semiempirical formula

$$\frac{D_s}{D_0} = (1 - 1.56\phi)(1 - 0.27\phi) \tag{19}$$

proposed originally by Lionberger and Russel.[46] This formula conforms overall well, up to $\phi \approx 0.3$, with the exact second-order virial form[47]

$$\frac{D_s}{D_0} = 1 - 1.832\phi - 0.219\phi^2 + \mathcal{O}(\phi^3). \tag{20}$$

For volume fractions exceeding 0.3, the second-order virial expansion is less accurate.[20]

The hydrodynamic function is a true short-time property on the colloidal time scale. Simulation results for the mean-

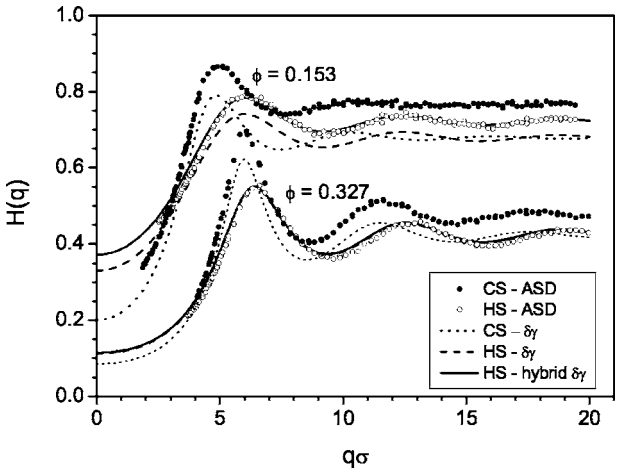

FIG. 4. ASD-$H(q)$, zeroth-order $\delta\gamma$-$H(q)$, and hybrid $\delta\gamma$-ASD $H(q)$ for $\phi = 0.327$ (sample 2: lower set of curves) and $\phi = 0.153$ (sample 5: upper set of curves), respectively. Comparison between charged spheres (CSs) and neutral hard spheres (HSs). The system parameters are as in Fig. 3.

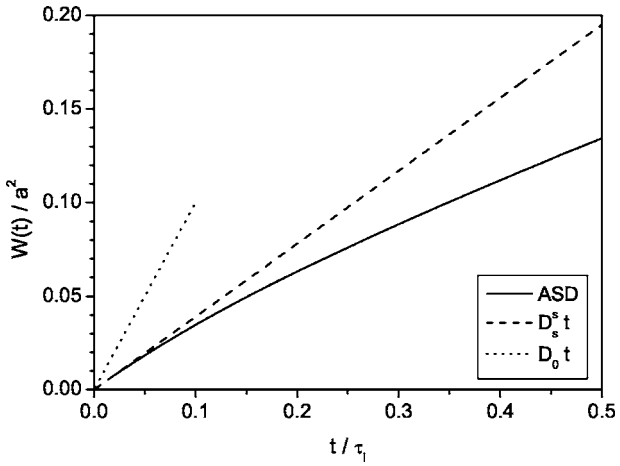

FIG. 5. ASD simulation results, using $N=216$ particles, for the mean-squared displacement $W(t)/a^2$ vs reduced time t/τ_I for $\phi=0.327$ and $Z=28$. Additionally displayed is the short-time asymptotic form $D_s(Z,\phi)t$ (dashed line) in comparison with the mean-squared displacement of noninteracting spheres (dotted line).

squared displacement with time measured in units of the "interaction" time τ_I are depicted in Fig. 5 for $\phi=0.327$ and $Z=28$, i.e., for a system akin to sample 2. We note that the short-time self-diffusion coefficient of charged spheres is smaller than D_0, but larger than the coefficient for neutral spheres at the same density, as can also be seen from the large-q form of $H(q)$ in Fig. 4. Figure 5 nicely shows that the transition from short-time diffusion to sublinear diffusion occurs roughly for $t=\mathcal{O}(\tau_I)$.

After having analyzed the $\delta\gamma$-scheme predictions for $H(q)$ in comparison with ASD simulations, we will next interpret our SAXS, PCS, and NSE data for apoferritin in terms of the OMF model.

B. Comparison with experimental data

1. Static structure factor

The structure factors, $S(q)$, obtained using SAXS (Ref. 1) for five differently concentrated apoferritin samples in $10^{-5}M$ NaCl solution (samples 1–5 in Table I) have been fitted using the RY and RMSA integral equation schemes. The only adjustable parameter is the effective charge Z_{RY} or Z_{RMSA}, respectively, determined from a fit to the SAXS structure factor peak height. The parameters characterizing the five samples, and the fit charges, are listed in Table I. The SAXS data for $S(q)$, and the RY and RMSA fits (solid lines) are shown in Fig. 6. Notice that the RY and RMSA curves for $S(q)$ are practically indistinguishable within the experimentally scanned q range. The inset shows the calculated radial distribution functions $g(r)$ of samples 1, 3, and 5. It is interesting that the differences between the RY and RMSA fitting curves are more pronounced for the $g(r)$.

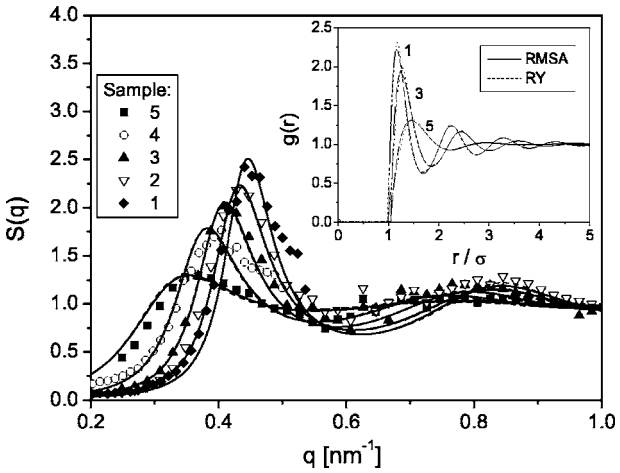

FIG. 6. RY/RMSA fit (solid lines) of the SAXS-determined static structure factors $S(q)$ (symbols) of apoferritin dispersions at five different protein concentrations (samples 1–5). The inset shows the RY/RMSA radial distribution functions of samples 1–3–5. The system parameters of samples 1–5, and the RY and RMSA fitting charges are listed in Table I.

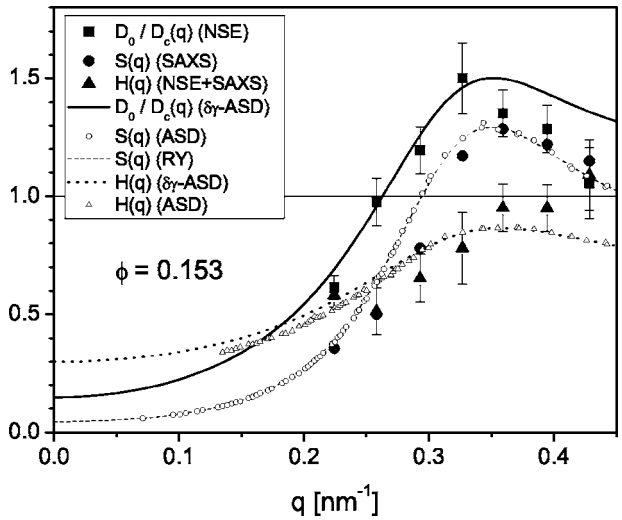

FIG. 7. NSE data for $D_0/D_c(q)$ of sample 5, reproduced from Ref. 3, in comparison with hybrid $\delta\gamma$-ASD results for $S(q)/H(q)$, with $S(q)$ calculated in RY approximation. The experimental $H(q)$ has been determined from the NSE-$D_c(q)$ using the SAXS data for $S(q)$. For completeness, the figures include further the finite-size corrected ASD result for $H(q)$ as shown already in Fig. 3.

Regarding the apoferritin solutions, the most interesting result in Table I is that the effective protein charges determined by RY and RMSA, respectively, increase monotonically with increasing protein concentration. The RMSA charges in Table I are larger than the RY charges since the RMSA underestimates the strength of the pair correlations. The RY charges, on the other hand, are practically identical to the charges determined by the ASD simulations, i.e., there is very good agreement between the corresponding RY and ASD structure factors for equal system parameters. The peculiar $Z(\phi)$ dependence will be discussed further in the following analysis of our PCS measurements of the collective diffusion coefficient.

2. Collective diffusion coefficient

As pointed out in Sec. II, the q dependence of the collective diffusion coefficient $D_c(q)$ of appoferritin is measurable using the neutron spin-echo technique. Figure 7 includes NSE data of sample 5 for the reciprocal diffusion coefficient $D_0/D_c(q)=S(q)/H(q)$, reproduced from Ref. 3. Considering the experimental errors, good overall agreement is observed with the calculated $S(q)/H(q)$. Here $S(q)$ is obtained from the RY approximation (cf. Fig. 2). The theoretical $H(q)$ has

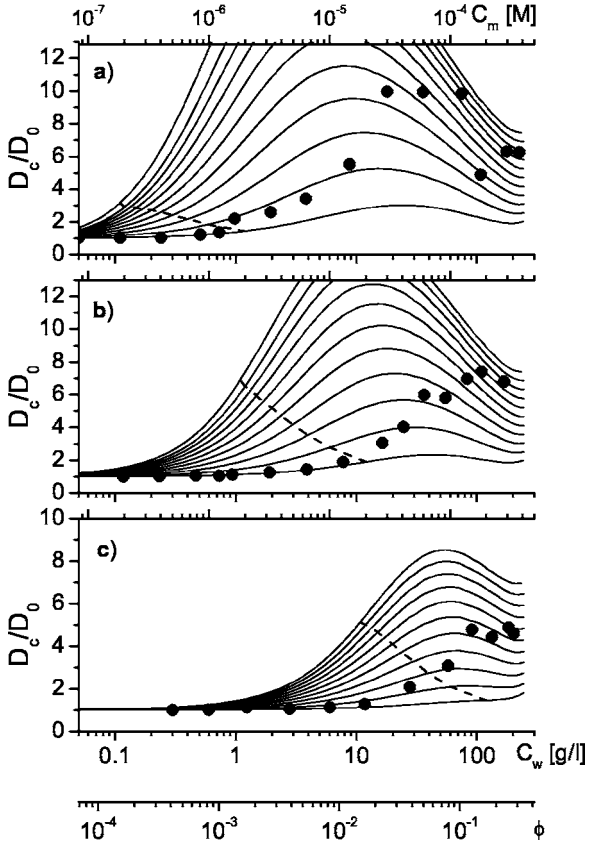

FIG. 8. Reduced short-time collective diffusion coefficient, D_c/D_0, vs protein weight concentration C_w, for apoferritin dispersions with (a) 10, (b) 100, and (c) 1000 μM of added NaCl. The filled circles are PCS data. The solid lines are zeroth-order $\delta\gamma$-scheme results using the RMSA input for $S(q)$, with effective protein charges 5, 10,…, 55e (from bottom to top). The remaining parameters are identical to those listed in Table I. The top axis gives the protein molar concentration, C_m, and the bottom axis displays the estimated volume fraction of hydrated proteins. The dashed line separates the salt counterion-dominated regime, where $n_s > n_{ci} \equiv n|Z|$, from the regime $n_s < n_{ci}$ which is dominated by counterions released from the protein surfaces.

been calculated using finite-size corrected ASD simulations and the hybrid $\delta\gamma$-ASD scheme discussed already in the context of Fig. 3. The experimental data for $H(q)$ have been obtained from dividing the NSE data of $D_c(q)$ by the SAXS data of $S(q)$.

Using PCS we have measured the (zero-q) collective diffusion coefficient, D_c, of apoferritin proteins in solutions with 10^{-5}, 10^{-4}, and $10^{-3}M$ added NaCl. The experimental data points for D_c are shown in Fig. 8, and compared with $\delta\gamma$-scheme results where the RMSA input has been used for numerical simplicity. The theoretical calculations have been performed for effective charge values of $5e, 10e, \ldots, 55e$, assumed to be independent of the protein concentration (solid lines from bottom to top). All curves for D_c calculated using the $\delta\gamma$ scheme exhibit a distinct maximum in $D_c(\phi)$ which increases (decreases) and shifts to smaller (larger) values of ϕ with increasing protein charge (salt content). To understand this behavior we remark that both $S(q=0)$ and $H(q=0)$ decrease with increasing ϕ. This is due to a concentration-induced reduction in the osmotic compressibility and in the sedimentation velocity. At smaller ϕ, $H(q=0)$ decreases less strongly than $S(q=0)$ leading thus to an increase in $D_c(\phi)$. When ϕ is increased, the hydrodynamic hindrance, as quantified by $H(q=0)$, eventually overcompensates the electrosteric protein repulsion so that D_c attains a maximum. The maximum in $D_c(\phi)$ becomes smaller with increasing salinity since the osmotic compressibility is increased.

Although the PCS data also show a maximum in the ϕ dependence of D_c for the two lower concentrations of added salt [cf. Figs. 8(a) and 8(b)], it is apparent that the data points cannot be described consistently by any of the fixed-charged theoretical curves. This is similar to the SAXS experiments where the static structure factors cannot be fitted theoretically assuming a concentration-independent effective protein charge.

3. Comparison with the coupled-mode theory

In previous work,[1] some of the present authors have applied the so-called CMT to interpret the same data for the collective protein diffusion coefficient. The simplified version of the CMT used in Ref. 1, however, neglects HI and includes $S(0)$ in a very simplified form. As a consequence, the observed maximum in $D_c(\Phi)$ cannot be explained in the framework of this theory. Furthermore, the values of the protein charge obtained from the CMT fits of D_c were lower than those obtained from the corresponding $\delta\gamma$-scheme fits. Since variants of the CMT have been used by several authors[48–53] to describe collective diffusion, it is worthwhile to discuss its relation with the present one-component approach.

The coupled-mode approach explicitly considers, within certain approximations, the coupling of the dynamics of the polyion with the counterions and the added salt ions. The OMF model calculations presented in this work, which ignore this explicit dynamic coupling, make it possible to use a more general version of the CMT, referred to in the following as general coupled-mode theory (GCMT). The GCMT may be used to estimate corrections to our OMF model results for D_c. The basis of the GCMT is the more refined primitive model of many-component electrolytes.

In the zero-q limit, the collective diffusion coefficient of the macroion component 1 is approximated in GCMT as

$$D_c = D_c^{\mathrm{OMF}}(1 - C), \tag{21}$$

where $D_c^{\mathrm{OMF}} = H_{11}(q=0)/S_{11}(q=0)$ is the short-time collective diffusion, as calculated within the OMF model of dressed macroions on demanding that $H_{11} = D_0 H(0)$ and $S_{11} = S(0)$. The correction term C accounts for the noninstantaneous dynamics of small counterions (component 2) and coions (component 3) . It is given by[49,51]

$$C = \frac{\Sigma_{\alpha,\beta=1}^{3}(n_1 n_\beta)^{1/2} Z_\alpha Z_\beta H_{1\alpha} H_{1\beta}}{H_{11}\Sigma_{\alpha,\beta=1}^{3}(n_\alpha n_\beta)^{1/2} Z_\alpha Z_\beta H_{\alpha\beta}}. \tag{22}$$

For simplicity we have assumed here that the protein-surface dissociated counterions are identical to the added salt counterions. They can be treated thus as a single component 2. Furthermore, $H_{\alpha\beta} = D_s^\alpha \delta_{\alpha\beta} + H_{\alpha\beta}^d(q \to 0)$ are the zero-q partial hydrodynamic functions consisting of a distinct part $H_{\alpha\beta}^d$, and a self-part quantified by the short-time self-diffusion co-

efficient, $D_s^{(\alpha)}$, of component α.[8] The number density of component α is n_α, and Z_α is the bare ionic charge as specified within the primitive model. We reemphasize that the bare protein charge Z_1 is in general different from the effective protein charge Z used in the OMF model, with both charges being equal only in the limit of weak ionic interactions.

In the OMF model of dressed macroions interacting by the effective pair potential (1), the counter- and coions are assumed to be pointlike, and to respond to the motion of the macroions infinitely rapidly. In contrast with this, the small ion dynamics slows down the macroion diffusion, as described approximately by the attenuation term C. This term can be appreciably larger than zero at low salinities. It becomes equal to zero only for large macroions where the microions can be treated as pointlike and quasi-instantaneous in their dynamic response. The GCMT result (22) is based on a short-time normal-mode expansion of the matrix of partial dynamic structure factors $S_{\alpha\beta}(q,t)$, with the fastest so-called Debye or overdamped plasmon mode being projected out. As a consequence, the GCMT does not account for microionic long-time relaxations which are also referred to as memory effects. In steady-state situations, the relaxation effect describes a small distortion from spherical symmetry of the microionic cloud around a macroion. The electrolyte friction felt by a single charged colloidal particle translating through an electrolyte solution is an example of such a relaxation effect not described by the GCMT.[12,50,54,55] In fact, for nonzero added electrolyte the attenuation term C in Eq. (22) reduces to zero for $n_1 \to 0$.

In applications of the GCMT to charged biopolymers and micelles,[48,49,52,53] an additional approximation is introduced by considering only macroion-macroion hydrodynamic interactions. Then, Eq. (22) simplifies to

$$C = \frac{n_1 Z_1^2 D_0 H(0)}{n_1 Z_1^2 D_0 H(0) + (n_2 Z_2^2 D_0^{(2)} + n_2 Z_3^2 D_0^{(3)})}, \tag{23}$$

with $D_0^{(\alpha)}$ denoting the diffusion coefficient of an α-type microion at infinite dilution. It should be noted here that static microion-microion and protein-microion correlations enter in Eq. (22) only implicitly through the nonideal parts of the partial hydrodynamic functions associated with the microions. These hydrodynamic parts are here disregarded, which explains why C in Eq. (23) is independent of these static correlations. Whereas the neglect of microion-microion HI can be justified to a certain extent,[55] disregarding protein-microion HI is a more severe approximation for the significantly charged proteins considered in this paper. Recent theoretical calculations have revealed that macroion-microion HIs are essential for the electrolyte friction effect.[54,55]

Notwithstanding these cautioning remarks, we may use Eq. (23) for a rough estimate of the correction to the OMF-D_c caused by the small ions dynamics. Such an estimate is presented in Fig. 9, which includes a plot of C versus the protein weight concentration, C_w, for various added salt concentrations. In the calculation of C according to Eq. (23), we have assumed monovalent counter- and coions of equal free diffusion coefficients. The OMF collective diffusion coefficient is determined for calculational simplicity by the $\delta\gamma$ scheme with the RMSA input for $S(q)$, using a constant effective protein charge of $Z_{\mathrm{RMSA}}=20$ (from Fig. 11 we conclude here that $Z_{\mathrm{RY}} \approx Z_{\mathrm{RMSA}}$). Moreover, the bare protein charge Z_1 in the primitive model is estimated by Z_{RY}. Given the severe approximations made for Eq. (23), we can ignore here the distinction between bare and effective charges, which frees us from specifying such a relationship. The relation between bare and effective charges of liquidlike dispersions of correlated macroions is a difficult and long-standing problem which is still not satisfactorily solved.

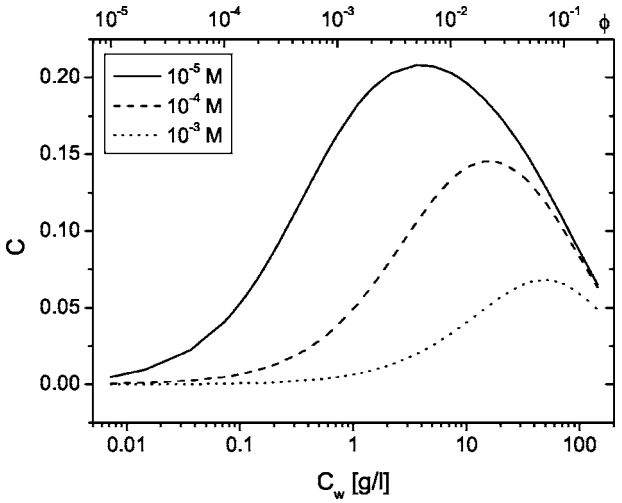

FIG. 9. Collective attenuation parameter C determined from the GCMT [Eq. (23)], vs protein weight concentration and protein volume fraction for three concentrations of added NaCl as indicated in the figure. The OMF collective diffusion coefficient is calculated using the $\delta\gamma$ scheme with RMSA input for a fixed effective protein charge of $Z_{\mathrm{RMSA}}=20$. For simplicity, the bare protein charge is approximated by Z_{RMSA}. The counter- and coions are assumed to be monovalent with identical free diffusion coefficients $D_0^{(2)}=D_0^{(3)}=1.5\times10^{-5}$ cm^2/s. The Stokesian free diffusion coefficient of proteins is $D_0=3.1\times10^{-7}$ cm^2/s.

As seen from Fig. 9, C becomes increasingly important as the salt concentration decreases, rising to a maximum of about 20% for the lowest salt concentration of $10^{-5}M$ NaCl studied in this work. The maximum in C is due to the concentration dependence of the OMF input for $H(0)$. Without protein-protein HI, i.e., for $H(0)=1$, C would increase monotonically with increasing protein concentration. The growth in C as a function of C_w is less pronounced for a larger salt content. With HI considered, however, $H(0)$ becomes a monotonically decreasing function in C_w giving rise to a single maximum in C as a function of protein concentration. The location of this maximum is different from that of the maximum in the corresponding OMF-D_c (cf. Fig. 8). We conclude this digression on the GCMT by emphasizing that a more quantitative analysis of small ion dynamic effects on the collective diffusion of macroions should include memory effects and macroion-microion HI. Work in this direction, which builds on a mode-mode coupling scheme with HI included, is in progress.[56]

4. Effective protein charge and Debye screening length

Both from the OMF calculations presented here for $S(q)$ and D_c and from the former CMT estimates in Ref. 1, we are

led to the conclusion that the effective charge of apoferritin is an increasing function of the protein concentration, at least for the three relatively small salt concentrations considered here.

In order to understand this phenomenon, we compare the number density, $n_{ci}=n|Z|$, of counterions released from the protein surfaces with the number density, n_s, of added salt counterions. Figure 8 shows the dashed line where $n_{ci}=n_s$, i.e., where $\kappa_{ci}=\kappa_s/\sqrt{2}$. The region to the left from this line represents systems with $n_s > n_{ci}$.

Consider now a system with zero added salt. Here the effective charge of proteins is determined only by the dissociation constant of surface counterions. Adding salt as a source of new ions with the binding constant (presumably) different from that of the surface counterions changes this picture dramatically. Depending on the amount of added salt and the difference in binding constants, some of the charged sites may be neutralized by the bounded salt ions. As a result, the effective charge of the particle will decrease with increasing added salt concentration until equilibrium is reached. Further increase of the added salt concentration will not change the effective charge. We can also consider adding colloidal particles to a solution of given salt concentration. For small particle concentrations, we expect small effective charge values for the colloidal particles, similar in magnitude to those at very high added salt concentrations, because in both cases most of the charged surface sites can be neutralized by the salt ions. On increasing the particle concentration, we finally reach the point at which the number of protein charge sites exceeds the number of available salt ions. Then the effective particle charge will start to increase up to the level determined by the binding constant of the counterions.

This qualitative mechanism is reflected in our experimental data. It is apparent from Fig. 8, by looking from the low-concentration side, that the data points start deviating from the $Z=5$ line almost exactly at the point marked by the dotted line. Only for the highest salt concentration do deviations emerge at smaller protein concentrations. The explanation for this discrepancy might be a change of the sodium ion binding constant with ionic strength. It has been found in earlier work on proteins that the binding constants of added metal ions (i.e., Na^+ in our case) depend upon the ionic strength of the solution.[57] At higher ionic strength, the stronger screening of electrostatic forces reduces the binding affinity because the counterions have to come closer to be trapped by the protein surface. This effect was observed both when the increase in the ionic strength resulted from the addition of salt, and from an increase in the protein concentration (with increased contribution of counterions to the ionic strength). As a result, the effective charge of the proteins increases with the ionic strength.

In order to quantify the $\delta\gamma$-scheme analysis results of the PCS data for each experimental point in Fig. 8, we have determined an effective charge Z_{RMSA} by fitting the $\delta\gamma$-D_c to the experimental value. Knowing that the effective charge is usually overestimated in RMSA, we have calculated the associated, and very accurate, effective charge Z_{RY} by matching the Rogers-Young $S(q)$ to the RMSA structure factor.

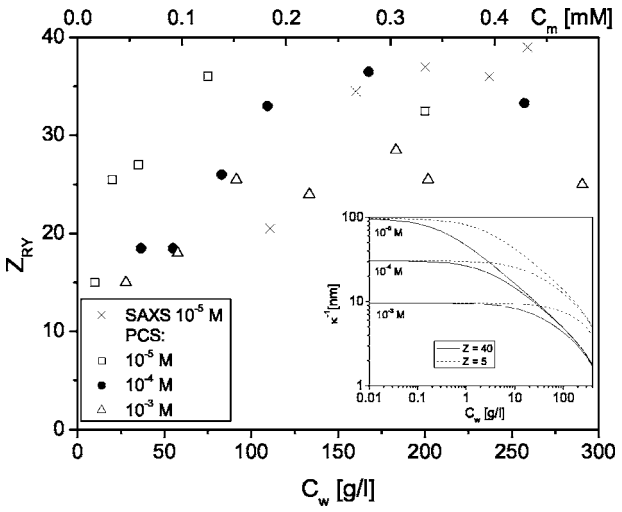

FIG. 10. Effective apoferritin charge number vs protein weight concentration, calculated from the RY fit to the SAXS-$S(q_m)$ and to the PCS-D_c. The inset shows the concentration dependence of the Debye-Hückel screening length for two different charges.

The values for Z_{RY} obtained in this way for the PCS data are plotted in Fig. 10 as a function of the protein weight concentration, C_w, and the corresponding molar concentration, C_m, of proteins. However, since this procedure can be performed only for conditions at which the primary peak in $S(q)$ is clearly visible, the range of lowest concentrations is not represented in this plot. In Fig. 10 we also show the effective charges derived from the SAXS data analysis listed in Table I (crosses). The increase of Z with increasing protein concentration for all samples is clearly visible from this figure for a concentration range up to $\sim$100 g/l. Above this concentration the value of Z appears to saturate, as expected from our former considerations. For the lowest added salt concentration of $10^{-5}M$, the saturation of Z is reached at lower protein concentration. This finding is consistent with our explanation given above.

As noted before, increasing the ionic strength reduces the specific ion binding affinity of proteins. Therefore, it is interesting to estimate how the ionic strength depends on the protein concentration. The ionic strength can be easily expressed in terms of the Debye screening length κ^{-1}. The value of κ^{-1} determines also the range and, to some extent, the strength of electrostatic interactions. The inset of Fig. 10 quantifies the decrease in κ^{-1} with increasing apoferritin concentration. The values of κ^{-1} have been calculated selecting a small and a large protein charge, respectively, namely, $Z_{RY}=5$ and 40. For a given Z, the Debye screening lengths of all three salt concentrations considered converge with increasing protein concentration, since the screening becomes increasingly dominated by the surface-released counterions [cf. Eq. (2)]. For the highest protein charge $Z=40$ considered, this convergence occurs at a smaller C_w, since there are more counterions released from the protein surfaces.

It is thus easy to comprehend that the calculated and experimental values for $D_c(\phi=0.3)$ displayed in Fig. 8 are quite similar for all three NaCl concentrations; for a protein concentration as large as $\phi=0.3$, κ^{-1} is practically determined by the counterions released from the protein surfaces.

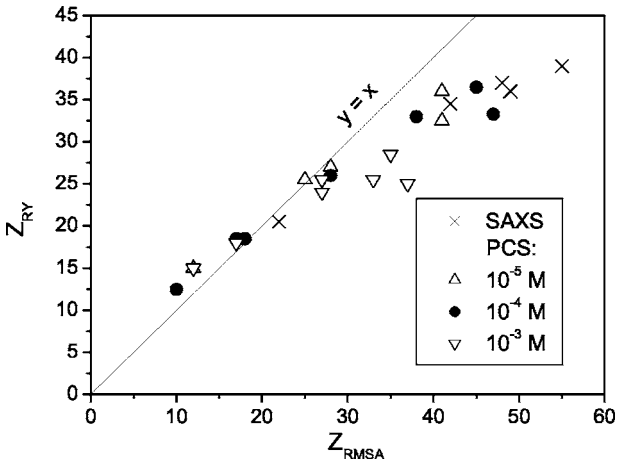

FIG. 11. Relationship between the effective charge numbers in the RY approximation and the RMSA that leads to identical principal peak heights of $S(q)$.

As a side result of our calculations of the effective apoferritin charges, we have obtained an interesting relation between Z_{RMSA} and Z_{RY}, which is depicted in Fig. 11. For smaller values of Z, both charges are roughly equal to each other, whereas $Z_{\mathrm{RY}} < Z_{\mathrm{RMSA}}$ is observed when the effective charge exceeds about 30. Of course, this crossover value will change when the particle size or other system parameters are varied.

V. CONCLUDING REMARKS

Previously measured collective diffusion coefficients at zero and finite values of q, and equilibrium static structure factors of dense apoferritin solutions at low to moderate salinities have been used to test recently developed one-component macroion-fluid-based short-time calculations for concentrated dispersions of charged colloidal spheres. Moreover, a former CMT analysis of collective protein diffusion was confronted with the OMF model-based theoretical and computer simulation results. For $S(q)$ we have shown that the q dependence of the experimental structure factors is quantitatively reproducible on the basis of a simple OMF model of dressed spherical macroions. From our structure factor analysis we have found that the effective protein charge is a function of the protein concentration. The ϕ dependence of Z can be attributed to the balance between the number of charged sites on the proteins' surface and the number of available sodium ions and, probably to a much lesser degree, to the ionic-strength dependence of the surface binding constants of added sodium ions.

The ϕ dependence of the collective diffusion coefficient at various salt contents was analyzed, again within the simple OMF model, using the $\delta\gamma$ approximation scheme in combination with an integral equation input for $S(q)$. We have performed accelerated Stokesian dynamics computer simulations to assess the accuracy of this scheme for charge-stabilized colloids. We have found that even for dense systems, the q-dependent distinct part of the hydrodynamic function, and the general trends for $H(q)$, well described by the $\delta\gamma$ scheme. However, the self-part, D_s, of the computer-simulated $H(q)$ is underestimated. This finding implies that the actual effective protein charges derived from the PCS measurements of D_c are actually somewhat smaller than the $\delta\gamma$-scheme values of Z depicted in Fig. 8. The $\delta\gamma$ scheme remains nonetheless very useful for predicting general trends in the behavior of D_c and $H(q)$, at least on a semiquantitative level. In principle, one can improve the accuracy of the $\delta\gamma$ scheme by combining it with accurate ASD calculations of D_s. However, such a hybrid scheme calculation requires a much larger numerical effort, in particular, when one needs to handle the data points of many systems. For dilute protein solutions, D_s can be determined more easily from an analytical pairwise-additivity scheme of the HI. We will study the collective diffusion of dilute apoferritin solutions in future work, both from experimental and theoretical points of view.

To summarize, the main objective of this work has been to investigate the applicability of the simplistic OMF model to describe static and diffusion properties of modestly salted apoferritin solutions. Our consistent analysis of apoferritin properties suggests that finer details of protein interactions such as discrete surface charge patterns and hydration forces are totally indispensable for an overall description only when protein solutions with larger amounts of added salt are considered.

ACKNOWLEDGMENTS

This work has been supported by the Deutsche Forschungsgemeinschaft (Transregio SFB-TR6) and the Polish-German Personnel Exchange Program (DAAD/KBN No. DB000177). Part of this work was done within the framework of the "SoftComp" Network of Excellence (No. S080118). Two of the authors (J.G.) and (A.W.) acknowledge support from the Polish Ministry of Scientific Research and Information Technology (Project No. 1 PO3B 008 28). Another author (A.J.B.) is a member of CONICET, Argentina, and acknowledges financial support from the Fundación Antorchas (Project 13927/3).

[1] W. Häussler, A. Wilk, J. Gapinski, and A. Patkowski, J. Chem. Phys. **117**, 413 (2002).
[2] W. Häussler, Chem. Phys. **292**, 425 (2003).
[3] W. Häussler and B. Farago, J. Phys.: Condens. Matter **15**, S197 (2003).
[4] F. J. Rogers and D. A. Young, Phys. Rev. A **30**, 999 (1984).
[5] J. P. Hansen and J. B. Hayter, Mol. Phys. **46**, 651 (1982).
[6] P. N. Pusey, in *Liquids, Freezing and Glass Transition II*, Les Houches Sessions 1989, edited by J.-P. Hansen, D. Levesque, and J. Zinn-Justin (North-Holland, Amsterdam, 1991), pp. 763–942.
[7] J. K. G. Dhont, *An Introduction to Dynamics of Colloids* (Elsevier, Amsterdam, 1996).
[8] G. Nägele, Phys. Rep. **272**, 215 (1996).
[9] W. B. Russel, D. A. Saville, and W. R. Schowalter, *Colloidal Dispersions* (Cambridge University Press, Cambridge, 1989).
[10] A. R. Denton, Phys. Rev. E **62**, 3855 (2000).
[11] S. Alexander, P. M. Chaikin, P. Grant, G. J. Morales, and P. Pincus, J. Chem. Phys. **80**, 5776 (1984).
[12] M. Tirado-Miranda, C. Haro-Perez, M. Quesada-Perez, J. Callejas-Fernandez, and R. Hidalgo-Alvarez, J. Colloid Interface Sci. **263**, 74 (2003).
[13] A. Diehl and Y. Levin, J. Chem. Phys. **121**, 12100 (2004).
[14] W. B. Russel and D. W. Benzing, J. Colloid Interface Sci. **83**, 163 (1981).
[15] M. Deserno and H. H. von Grünberg, Phys. Rev. E **66**, 011401 (2002).
[16] H. Löwen in *Soft Matter: Complex Materials on Mesoscopic Scales*, edited by J. K. G. Dhont, G. Gompper, and D. Richter (Schriften des Forschungszentrums Jülich, Julich, 2002), Vol. 10, pp. B17.1–B17.31.

[17] R. Klein, H. H. von Grünberg, C. Bechinger, M. Brunner, and V. Lobaskin, J. Phys.: Condens. Matter **14**, 7631 (2002).
[18] E. Allahyarov, H. Löwen, J. P. Hansen, and A. A. Louis, Phys. Rev. E **67**, 051404 (2003).
[19] J. P. Hansen and I. R. McDonald, *Theory of Simple Liquids*, 2nd ed. (Academic, London, 1986).
[20] G. Nägele, *The Physics of Colloidal Soft Matter*, Lecture Notes Vol. 14 (Institute of Fundamental Technological Research, Polish Academy of Sciences, Warsaw, 2004).
[21] R. B. Jones and P. N. Pusey, Annu. Rev. Phys. Chem. **42**, 137 (1991).
[22] P. Szymczak and B. Cichocki, Europhys. Lett. **59**, 465 (2002).
[23] E. Wajnryb, P. Szymczak, and B. Cichocki, Physica A **335**, 339 (2004).
[24] A. J. Banchio, G. Nägele, and J. Bergenholtz, J. Chem. Phys. **113**, 3381 (2000).
[25] C. W. J. Beenakker and P. Mazur, Phys. Lett. A **98**, 22 (1983).
[26] C. W. J. Beenakker, Ph.D. thesis, University of Leiden, 1984.
[27] U. Genz and R. Klein, Physica A **171**, 26 (1991).
[28] G. Nägele, O. Kellerbauer, R. Krause, and R. Klein, Phys. Rev. E **47**, 2562 (1993).
[29] G. Nägele, B. Steininger, and R. Klein, Phys. Scr., T **55**, 119 (1994).
[30] G. Nägele, B. Mandl, and R. Klein, Prog. Colloid Polym. Sci. **98**, 117 (1995).
[31] A. J. C. Ladd, H. Gang, J. X. Zhu, and D. A. Weitz, Phys. Rev. E **52**, 6550 (1995).
[32] P. N. Segrè, O. P. Behrend, and P. N. Pusey, Phys. Rev. E **52**, 5070 (1995).
[33] A. J. Banchio and G. Nägele (in preparation).
[34] A. J. Banchio and J. F. Brady, J. Chem. Phys. **118**, 10323 (2003).
[35] D. O. Riese, G. H. Wegdam, W. L. Vos, R. Sprik, D. Fenistein, J. H. H. Bongaerts, and G. Grübel, Phys. Rev. Lett. **85**, 5460 (2000).
[36] D. O. Riese, W. L. Vos, G. H. Wegdam, F. J. Poelwijk, D. Abernathy, and G. Grübel, Phys. Rev. E **61**, 1676 (2000).
[37] G. Grübel, D. Abernathy, D. O. Riese, W. L. Vos, and G. H. Wegdam, J. Appl. Crystallogr. **33**, 424 (2000).
[38] W. Härtl, J. Wagner, Ch. Beck, F. Gierschner, and R. Hempelmann, J. Phys.: Condens. Matter **12**, A287 (2000).
[39] A. J. Banchio, G. Nägele, and J. Bergenholtz, J. Chem. Phys. **111**, 8721 (1999).
[40] P. N. Segrè, S. P. Meeker, P. N. Pusey, and W. C. K. Poon, Phys. Rev. Lett. **74**, 1250 (1995).
[41] B. Cichocki, M. L. Ekiel-Jezewska, P. Szymczak, and E. Wajnryb, J. Chem. Phys. **117**, 1231 (2002).
[42] G. Nägele, J. Phys.: Condens. Matter **15**, S407 (2003).
[43] W. Härtl, Ch. Beck, and R. Hempelmann, J. Chem. Phys. **110**, 7070 (1999).
[44] A. J. C. Ladd, J. Chem. Phys. **93**, 3484 (1990).
[45] A. P. Philipse and A. Vrij, J. Chem. Phys. **88**, 6459 (1988).
[46] R. A. Lionberger and W. B. Russel, J. Rheol. **38**, 1885 (1994).
[47] B. Cichocki, M. L. Ekiel-Jezewska, and E. Wajnryb, J. Chem. Phys. **111**, 3265 (1999).
[48] P. Tivant, P. Turq, M. Drifford, H. Magdelenat, and R. Menez, Biopolymers **22**, 643 (1983).
[49] L. Belloni and M. Drifford, J. Phys. (Paris), Lett. **46**, L1183 (1985).
[50] K. S. Schmitz and J. M. Schurr, Annu. Rev. Phys. Chem. **37**, 271 (1986).
[51] J. M. Schurr, Chem. Phys. **111**, 55 (1987).
[52] P. Retailleau, M. Ries-Kautt, A. Ducruix, L. Belloni, S. J. Candau, and J. P. Munch, Europhys. Lett. **46**, 154 (1999).
[53] S. U. Egelhaaf, V. Lobaskin, H. H. Bauer, H. P. Merkle, and P. Schurtenberger, Eur. Phys. J. E **13**, 153 (2004).
[54] M. Kollmann and G. Nägele, Europhys. Lett. **52**, 474 (2000).
[55] M. G. McPhie and G. Nägele, J. Phys.: Condens. Matter **16**, S4021 (2004).
[56] M. G. McPhie and G. Nägele (in preparation).
[57] S. Linse, B. Jönsson, and W. J. Chazin, Proc. Natl. Acad. Sci. U.S.A. **92**, 4748 (1995).